



# A $^{13}\text{C}$ three-dimensional DQ-SQ-SQ correlation experiment for high-resolution analysis of complex carbohydrates using solid-state NMR



S. Chandra Shekar<sup>a</sup>, Wancheng Zhao<sup>a</sup>, Liyanage D. Fernando<sup>a</sup>, Ivan Hung<sup>b</sup>, Tuo Wang<sup>a,\*</sup>

<sup>a</sup> Department of Chemistry, Louisiana State University, Baton Rouge, LA 70803, USA

<sup>b</sup> National High Magnetic Field Laboratory, Tallahassee, FL 32310, USA

## ARTICLE INFO

### Article history:

Received 28 December 2021

Revised 16 January 2022

Accepted 17 January 2022

Available online 21 January 2022

### Keywords:

Solid-state NMR

3D CCC correlation

Structure determination

Carbohydrates

Fungi

Plant cell wall

## ABSTRACT

Complex carbohydrates are the key components of the protective cell walls of microbial pathogens and the bioenergy reservoir in plants and algae. Structural characterization of these polymorphic molecules requires assistance from multidimensional  $^{13}\text{C}$  correlation approaches. To facilitate the analysis of carbohydrate structure using solid-state NMR, we present a three-dimensional (3D)  $^{13}\text{C}$ - $^{13}\text{C}$ - $^{13}\text{C}$  experiment that includes a double-quantum (DQ) dimension and is thus free of the cube's body diagonal. The enhanced resolution supports the unambiguous resonance assignment of many polysaccharides in plant and fungal cell walls using uniformly  $^{13}\text{C}$ -labeled cells of spruce and *Aspergillus fumigatus*. Long-range structural restraints were effectively obtained to revisit our understanding of the spatial organization of plant cellulose microfibrils. The method is widely applicable to the investigations of cellular carbohydrates and carbon-based biomaterials.

© 2022 Elsevier Inc. All rights reserved.

## 1. Introduction

Three-dimensional (3D) experiments are a standard approach used in biomolecular solid-state NMR studies but have rarely been applied to biomaterials [1–3]. Baldus, Rienstra, and Hong have established a collection of 3D  $^{13}\text{C}$ - $^{13}\text{C}$ - $^{13}\text{C}$  (CCC) correlation experiments that flexibly combine the detection of single-quantum (SQ) and double-quantum (DQ)  $^{13}\text{C}$  chemical shifts with various polarization transfer schemes and frequency filters to fulfill the needs for resonance assignment and obtaining long-range structural restraints [4–7]. Such 3D correlation experiments also have the potential of assisting the identification of many coexisting polymers and understanding their spatial association in carbon-based biocomposites [8–10].

Indeed, recent NMR studies of plant cell walls have already benefited from the SQ-SQ-SQ CCC experiment (Fig. 1a). In 2011, the first 3D CCC spectrum of plant materials was collected on uniformly  $^{13}\text{C}$ -labeled primary cell walls of *Arabidopsis* seedlings, reporting numerous intermolecular cross peaks between cellulose and pectin [9]. This was the first set of consolidated molecular-level data that support the putative interactions between these two biopolymers. The results also led to a revised concept that the hemicellulose xyloglucan only interacts with cellulose at lim-

ited spots [9], which was later combined with biochemical evidence to build new conceptual models of primary plant cell walls [11–13]. In 2015, this experiment was extended to the investigation of secondary plant cell walls [10]. Demonstrated on the mature stems of the same model plant (*Arabidopsis thaliana*), the high-resolution data successfully revealed the conformational distribution of the hemicellulose xylan and the interconnectivity of different cellulose domains [10].

Currently, carbohydrate solid-state NMR has to rely on carbon-13 due to the highly restricted choice of NMR-active nuclei. Nitrogen-15 is widely used in protein studies but is only applicable to a small number of nitrogenated sugars present in nature. Proton detection and oxygen-17 studies have demonstrated their effectiveness in protein and material research [14–17], but both are still in the exploratory stage for carbohydrate studies [18–20]. Therefore, there is an urgent need for more versatile CCC experiments to assist the structural analysis of carbohydrate polymers.

Here we adapt the 3D DQ-SQ-SQ CCC experiment, a scheme first demonstrated by Baldus and coworkers [4], to investigate the structure and packing of carbohydrate polymers in cellular environments. After the J-INADEQUATE module [21,22], a Combined R2<sub>nv</sub>-Driven (CORD) [23,24] block was implemented (Fig. 1b). The consideration is that CORD is a broadband homonuclear correlation sequence that even functions well under fast MAS conditions; therefore, it should remain effective for future applications on high-field magnets under fast spinning. Also, CORD needs very

\* Corresponding author.

E-mail address: [tuowang@lsu.edu](mailto:tuowang@lsu.edu) (T. Wang).

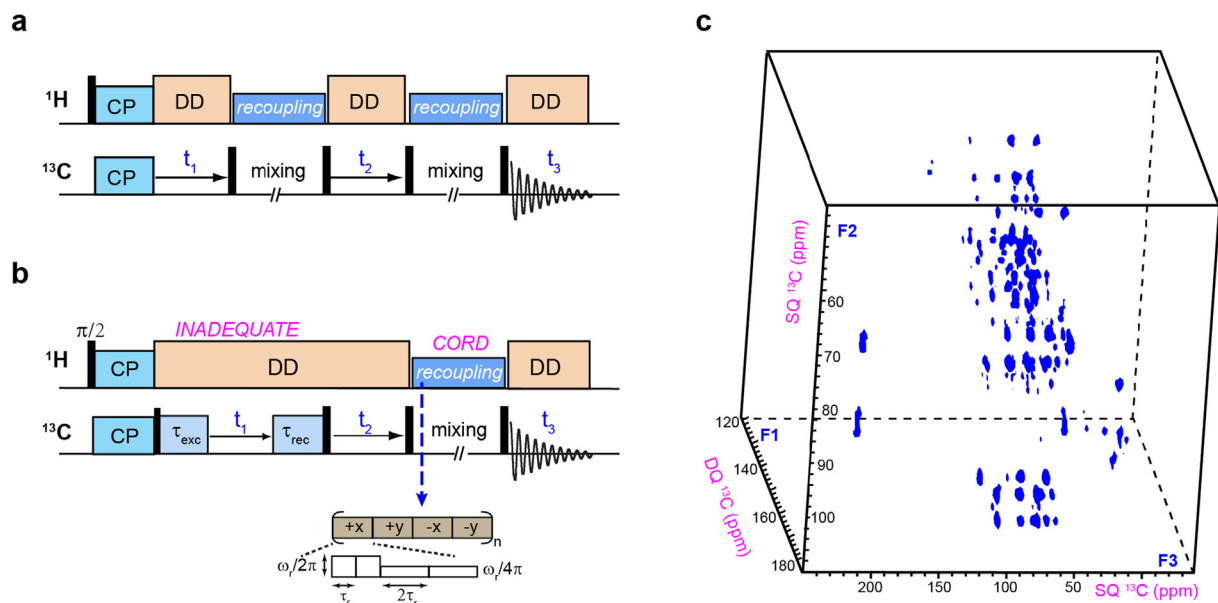


**Fig. 1.** 3D CCC experiments for characterizing carbon-rich biosolids. (a) 3D  $^{13}\text{C}$ - $^{13}\text{C}$ - $^{13}\text{C}$  correlation experiments relying on two  $^{13}\text{C}$ - $^{13}\text{C}$  mixing periods, for example, DARR/PDSD periods. (b) 3D  $^{13}\text{C}$ - $^{13}\text{C}$ - $^{13}\text{C}$  (DQ-SQ-SQ) experiment constructed as an INADEQUATE-CORD sequence. The INADEQUATE block is presented in a simplified format as it could be constructed using either J- or dipolar-based pulse sequence. The pulse program used for this study is provided in the [Supplementary Data](#). (c) Representative 3D INADEQUATE-CORD solid-state NMR spectrum collected on living cells of *A. fumigatus* at 800 MHz. The three dimensions (F1, F2, F3) report DQ, SQ, and SQ  $^{13}\text{C}$  chemical shifts, respectively.

low recoupling power as the radiofrequency (rf) field strength is only needed on the  $^1\text{H}$  channel and is matching only half of the spinning frequency during the majority (two-thirds) of the mixing period. This can effectively reduce the detrimental effect of rf power on sensitive biological samples such as the living cells of various organisms.

The unprecedented resolution provided by this 3D CCC (DQ-SQ-SQ) experiment allows us to systematically document the  $^{13}\text{C}$  chemical shift of various glucans and chitin molecules in the cell walls of a pathogenic fungus *Aspergillus fumigatus* [25,26], using its living cells. Signal multiplicity has been observed for chitin and  $\alpha$ -1,3-glucan; the former is attributed to the structural complexity of sugar units when placed in the hydrogen-bonded chitin microfibrils and the latter is correlated with the functional diversity of  $\alpha$ -1,3-glucans. The most rewarding improvement is on plant biomass, the research of which has long been hampered by insufficient resolution. We have resolved the signals of previously ambiguous carbon sites and further evaluated how different glucose conformers are packed in the bundled cellulose microfibrils. This experiment has shown its usefulness in the investigations of carbohydrate polymers and should facilitate the ongoing efforts in understanding the carbohydrate structure and assembly in algae, bacteria, fungi, plants, and human cells, as well as biomimetic materials [27–32]. The pulse program has been provided in the [Supplementary Data](#) to expedite future investigations.

## 2. Results and discussion

The 3D INADEQUATE-CORD spectrum of the 3-day-old *A. fumigatus* mycelium showed remarkable dispersion of the carbon peaks (Fig. 1c). The sample contains the living cells of this fungus, which should be a highly complex and challenging biosystem for NMR investigation. However, the outstanding spectral resolution (typically 0.3–0.7 ppm for  $^{13}\text{C}$  linewidths as reported recently) [33,34] allowed us to use it as a model system for cellular carbohydrates. The conventional INADEQUATE spectrum reports the signals from directly bonded carbons (Fig. 2a), and all the spin pairs of *A. fumi-*

*gatus* carbohydrates were marked using their DQ chemical shifts. As  $^1\text{H}$ - $^{13}\text{C}$  cross polarization was used for the creation of initial magnetization, the signals detected here mainly originated from four carbohydrate polymers found in the rigid portion of fungal cell walls (Fig. 2b). These molecules include chitin,  $\alpha$ -1,3-glucan,  $\beta$ -1,3-glucan (occasionally with  $\beta$ -1,6-linkage for branching), and the mixed linked  $\beta$ -1,3/1,4-glucan, which is a terminal segment of the diversely linked  $\beta$ -glucan network [35–37].

The implementation of a 53-ms CORD mixing period after the INADEQUATE block allowed the  $^{13}\text{C}$  magnetization to be transferred to all carbon sites in a molecule that showed up at a given double-quantum chemical shift (Fig. 3a). For example, the  $\beta$ -1,3-glucan carbon 1 and carbon 2 (B1 and B2) have single-quantum (SQ) chemical shifts of 103.6 ppm and 74.4 ppm, respectively. Therefore, in the INADEQUATE spectrum, their signals showed up at the double-quantum (DQ) chemical shift of 178 ppm, which is the sum of the two SQ chemical shifts. When CORD is implemented, the other carbons of  $\beta$ -1,3-glucan (B3, B4, B5, and B6) also appeared in the same DQ line, with well-resolved signals for resonance assignment.

Such a spectral feature confers an unique advantage over the conventional 2D correlation spectrum. Both the DQ-SQ correlation (such as INADEQUATE) and SQ-SQ correlation (such as DARR and CORD) spectra often have highly crowded regions, where the carbon connectivity cannot be explicitly tracked. For example, the carbon 1 signals of chitin and  $\beta$ -1,3-glucan are almost identical; therefore, their C1-CX (CX denotes other carbons) cross peaks are severely overlapped signals in the CORD spectrum (Fig. 3b). However, their C1-C2 spin pairs have distinct DQ chemical shifts: 159 ppm for chitin C1-C2 and 178 ppm for  $\beta$ -1,3-glucan C1-C2 as shown in Fig. 3a. Therefore, we can unambiguously resolve and assign all their carbon signals in the collapsed INADEQUATE-CORD spectrum, which is free of diagonal and has better dispersion of signals as benefited from the implementation of a DQ dimension.

When a DQ chemical shift contains only a single pair of carbons, all the carbon sites in the same molecule can be well resolved in the third dimension (Fig. 4a and [Supplementary Fig. 1](#)). For exam-

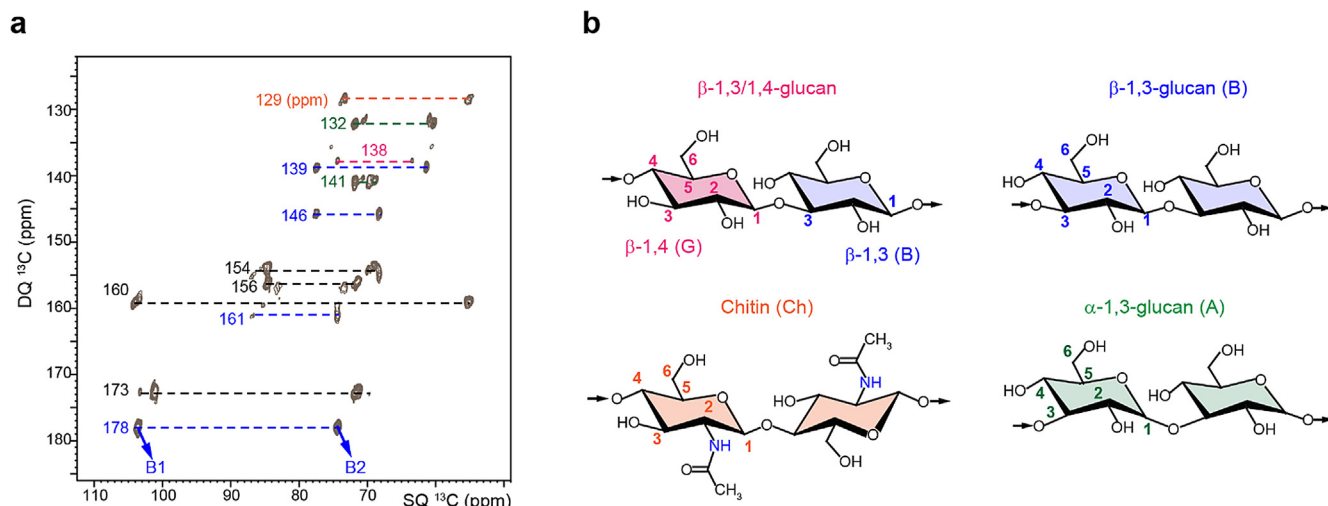


**Fig. 2.** 2D spectra of fungal cell wall carbohydrates. (a) 2D  $^{13}\text{C}$ - $^{13}\text{C}$  INADEQUATE (DQ-SQ) spectrum of *A. fumigatus* cells. Key cross sections are marked using the DQ  $^{13}\text{C}$  chemical shifts. (b) Representative *A. fumigatus* carbohydrates with the NMR abbreviations labeled. All carbohydrates are color-coded, and the color scheme is used for all fungal figures.

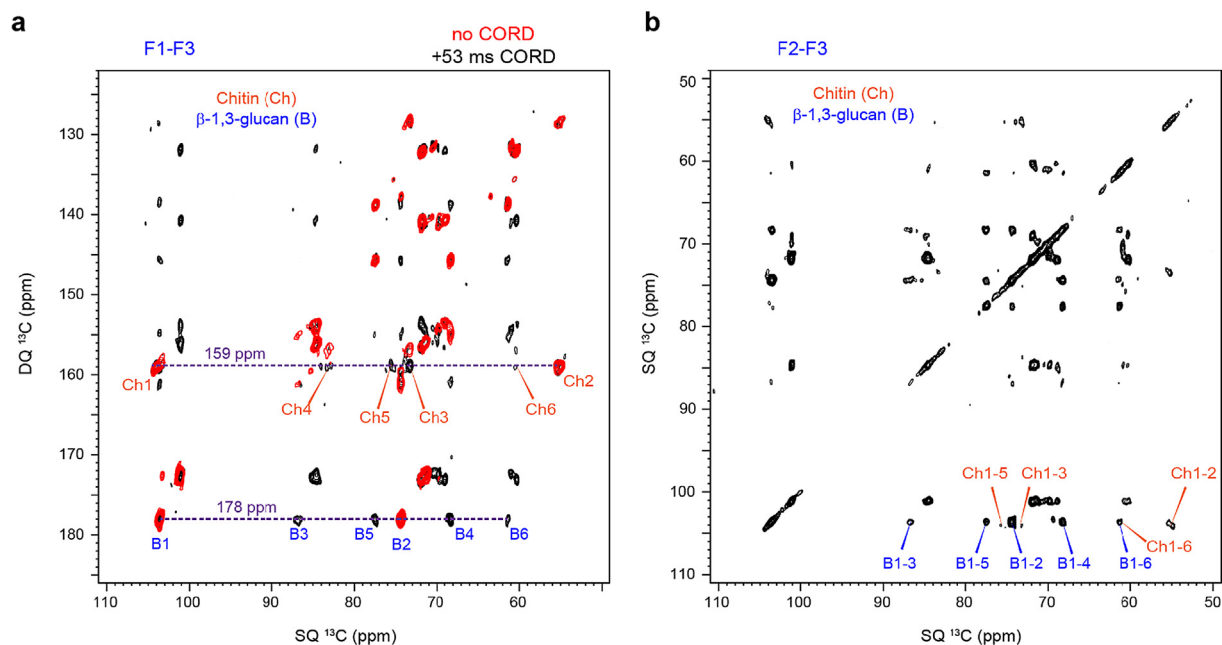


**Fig. 3.** Collapsed 2D spectra of the 3D INADEQUATE-CORD experiment. The 2D spectra plotted in black represent all the signals of the 3D INADEQUATE-CORD when being projected to (a) the F1-F3 dimensions and (b) the F2-F3 dimensions. For comparison, a conventional INADEQUATE spectrum (red) is overlaid with the F1-F3 plane, where the extra signals are from multi-bond intramolecular correlations within each molecule. The representative signals of chitin (Ch) and  $\beta$ -1,3-glucan (B) are labeled. For example, Ch1 denotes chitin carbon 1.

ple, in the F2-F3 plane at F1 = 178 ppm, both B1 and B2 will have cross peaks with the other carbons in  $\beta$ -1,3-glucan. Similar spectral patterns were also observed in other F2-F3 panels of this molecule, regardless of the F1 DQ chemical shifts, which provided confidence to the resonance assignment. The  $\beta$ -1,4-linked glucose units only account for a minor portion of the  $\beta$ -glucan matrix because the  $\beta$ -1,3/1,4-glucan constitute approximately 10% of all  $\beta$ -glucans [38]. It is not surprising that  $\beta$ -1,4-linked glucose residues have been particularly difficult to track using NMR. However, its  $^{13}\text{C}$  signals can be assigned using the F2-F3 plane extracted at F1 = 138 ppm.

Both  $\alpha$ -1,3-glucan and chitin showed peak multiplicity, with multiple sets of signals for each carbon. This observation further correlates with the functional diversity and structural complexity

of these biomolecules. Recent studies have revealed that  $\alpha$ -1,3-glucan is widely distributed in all functional domains of fungal cell walls, including the rigid and mobile portions (from the physical perspective) of both the alkali-soluble and alkali-insoluble fractions (from the chemical view) [33,34]. Differently, chitin has complex structural environments in the hydrogen-bonded microfibrils, which has been recently revealed by solid-state NMR and principal component analysis [39].

It is expected that a single DQ chemical shift might represent multiple pairs of carbon. For example, the 160 ppm DQ chemical shift is the sum of 104 ppm and 56 ppm from chitin C1 and C2, as well as 85 ppm and 75 ppm from the C4 and C5 of  $\beta$ -1,4-linked glucose units (Fig. 4b). All the  $^{13}\text{C}$  signals are well resolved even in the mixed planes, for example, those with concurrent con-

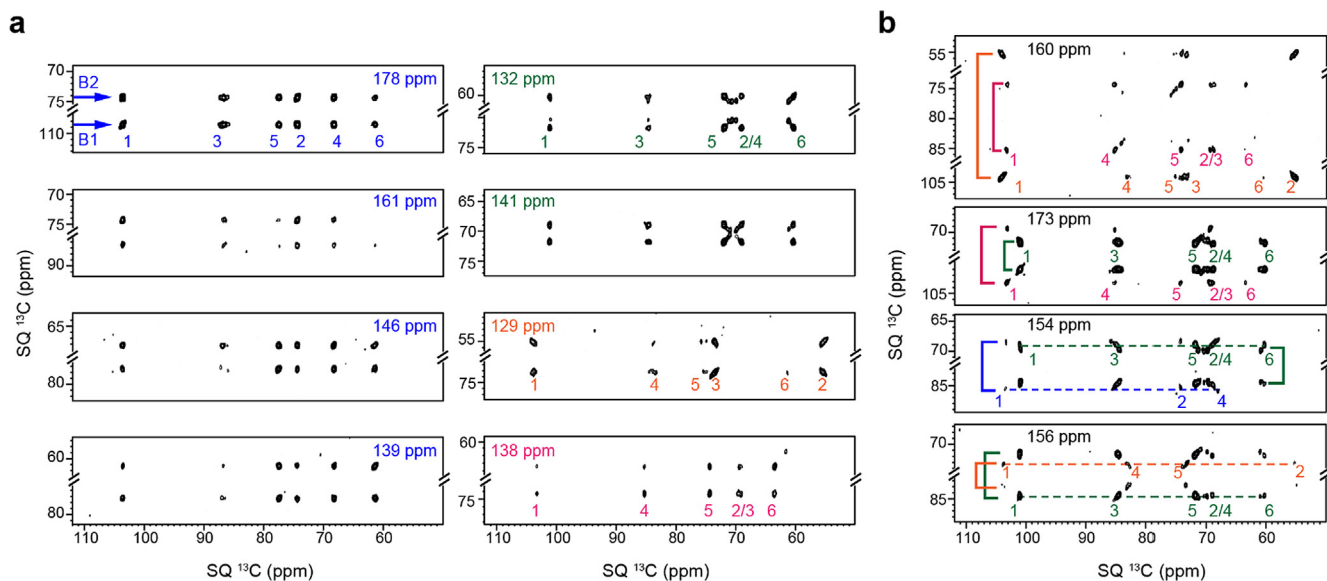


**Fig. 4.** 2D planes of the 3D spectra resolving signals of fungal cell wall carbohydrates. The double quantum  $^{13}\text{C}$  chemical shifts (in ppm) are marked in panels (a) and (b) to match the signals in Fig. 2a. (a) Well-resolved F2-F3 planes extracted from 3D INADEQUATE-CORD (DQ-SQ-SQ) spectrum of the *A. fumigatus* sample. The left panels show signals of  $\beta$ -1,3-linked glucans or glucose units (blue) while the right panel shows  $\alpha$ -1,3-glucan (green), chitin (orange), and  $\beta$ -1,4-linked glucose residues (magenta). The numbers (1–6) indicate the carbon numbers in each carbohydrate molecule as presented in Fig. 2b. Two arrows are used to annotate the lines of peaks for  $\beta$ -1,3-glucan carbon 1 (B1) and carbon 2 (B2), with correlations to each of the six carbons in this molecule. (b) F2-F3 planes with multiple molecules observed in each 2D plane. The full views of these panels are presented in Supplementary Fig. 1.

tributions from chitin and  $\beta$ -1,3/1,4-glucan ( $F1 = 160$  ppm),  $\beta$ -1,3/1,4-glucan and  $\alpha$ -1,3-glucan ( $F1 = 173$  ppm),  $\beta$ -1,3-glucan and  $\alpha$ -1,3-glucan ( $F1 = 154$  ppm), as well as chitin and  $\alpha$ -1,3-glucan ( $F1 = 156$  ppm). It is obvious that the unprecedented resolution offered by the 3D should facilitate the NMR studies of carbohydrate-rich biomaterials.

This 3D CCC experiment is particularly useful for the analysis of highly complex biosystems, such as plant secondary cell walls, whose spectra are much more congested than those of the fungal cells. Even the collapsed 2D INADEQUATE-CORD spectrum measured on a spruce stem sample failed to provide sufficient resolution for resolving a large number of carbohydrate units and conformers present in the cellulose microfibrils and matrix polysaccharides (Supplementary Fig. 2). However, the F2-F3 planes extracted at  $F1 = 138$  ppm (cellulose carbon 5 and 6) and  $F1 = 178$  ppm (cellulose carbon 1 and carbon 2) efficiently separated the many carbon peaks in the glucan chains residing on the surface or the internal domains of cellulose microfibrils (Fig. 5a). Matrix polysaccharides exhibited even better resolution ( $F1 = 174$  ppm) as benefited from their partial mobility.

We further differentiated the signals from the hydrophobic ( $s^g$ ) and hydrophilic ( $s^f$ ) chains of cellulose surface, the deeply embedded core chains ( $i^c$ ), and an intermediate layer ( $i^a$  and  $i^b$ ) bridging the core and the surface (Fig. 5b). These glucose units have been recently identified using high-resolution 2D  $^{13}\text{C}$ - $^{13}\text{C}$  correlation spectra [40], with their hydroxymethyl conformations restrained by  $^1\text{H}$ - $^1\text{H}$  distance measurements [41]. However, the peak congestion of these glucose units caused ambiguity in the previous efforts to complete the resonance assignment [40]. The resolution presented by the well-isolated signals, such as these C6-C1 cross peaks, has never been realized before. We can even resolve the carbon 2 signals of internal and surface chains that are apart by less than 0.5 ppm, which is below the  $^{13}\text{C}$  FWHM of individual cellulose peaks (0.7–1.0 ppm).

Although the spectrum is diagonal-free considering the 3D cube's body as shown in Fig. 1c, the diagonals and anti-diagonals of the 2D F2-F3 planes are clearly visible (Fig. 6), arising only from

the correlated spins in F3-F2 plane at a given  $F1$  (DQ) frequency, as has been noted by Baldus and co-workers [4]. For example, Fig. 6 shows the resonance assignment of all signals observed in the 2D plane extracted at  $F1 = 138$  ppm, which is the DQ chemical shifts of interior cellulose C5-C6 and surface cellulose C5-C6 carbon pairs. Therefore, diagonal signals can only be observed for C6-C6 and C5-C5 signals in the type-f and type-g surface chains as well as different types of interior residues. However, these diagonal signals differ from those of the conventional 2D SQ-SQ correlation spectra where all carbon sites present in the biosystem have their corresponding diagonal peaks. The diagonal signals observed in an F2-F3 plane of a 3D are more discrete as they only originate from the carbons selected by the DQ chemical shift (for example, only cellulose C5 and C6 here). Many other carbon sites in matrix polysaccharides have similar SQ chemical shifts but they are dispersed into different planes by their distinct DQ chemical shifts. Also, the diagonal does not leak across the whole spectral width (for example, 10–180 ppm for the  $^{13}\text{C}$  spectrum of plant cell walls) as typically observed in 2D correlation spectra. The DQ selection has clearly alleviated the spectral crowding issue.

A more promising application of this 3D experiment is to identify long-range correlations for structural determination. This was highlighted by the numerous intermolecular cross peaks revealed by the F2-F3 plane ( $F1 = 138$  ppm) of the 3D spectrum measured with a 300-ms long CORD mixing period. Site-specific and conformer-specific information of polymer packing can be obtained. For example, instead of simply reporting a cross peak between surface cellulose carbon 6 and interior cellulose carbon 4 ( $s6-i4$ ), we identified that the type-a and type-b glucose units ( $i^{a,b}$ ) were responsible for contacting the surface chains (Fig. 7). This observation perfectly aligns with the structural scheme presented in Fig. 5b, as  $i^{a,b}$  represents the layer of glucan chains that are directly underneath the surface chains. Always, two types of surface chains,  $s^f$  and  $s^g$ , were simultaneously involved in the cross peaks with internal chains (more specifically, the  $i^{a,b}$  chains), with comparable intensities. This is understandable as these two types of surface chains, regardless of their capability of retaining water

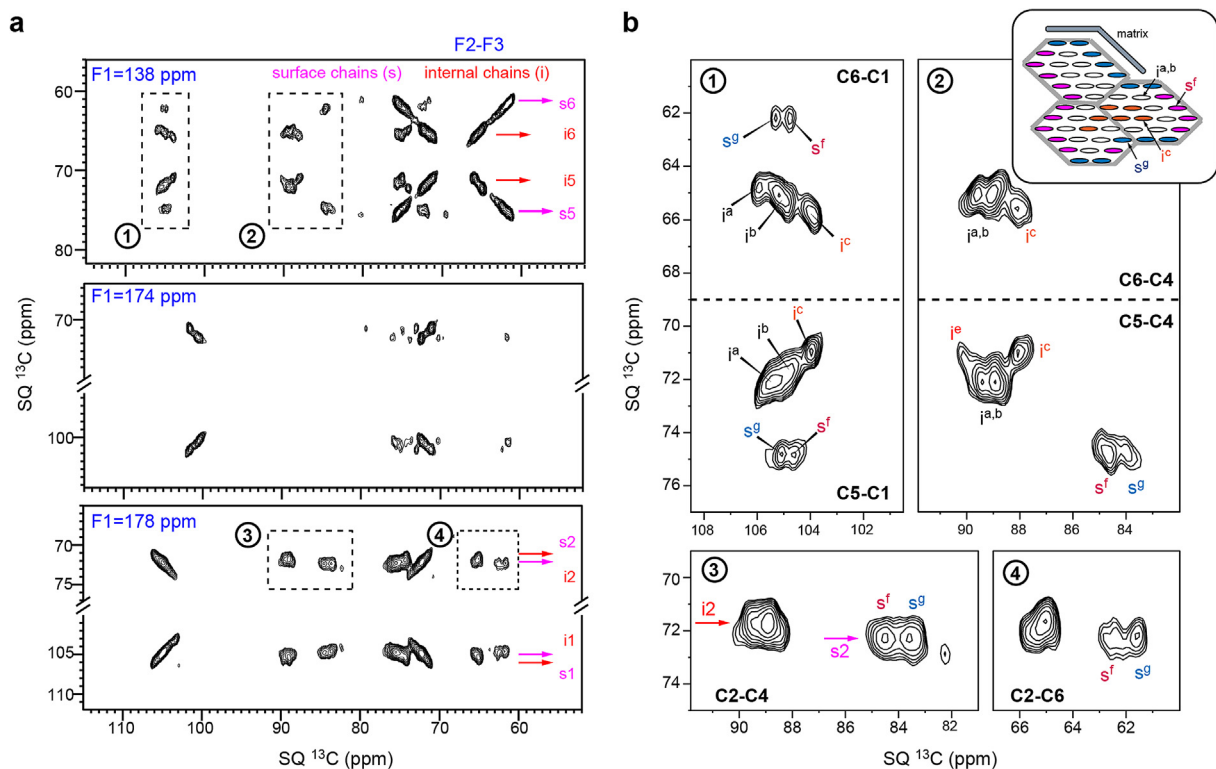


**Fig. 5.** 2D F2-F3 planes of spruce extracted from the 3D spectrum. (a) Representative planes of spruce cellulose (F1 = 138 ppm and 178 ppm) and matrix polysaccharides (F1 = 174 ppm). The rows of internal (i) and surface (s) chains are shown using arrows. (b) Zoom-in views of the numbered regions boxed by dashlines in panel (a). A bundle formed by three elementary cellulose microfibrils is shown to indicate the different packing environment for internal cellulose (types a, b, c) and surface chains (types f and g).

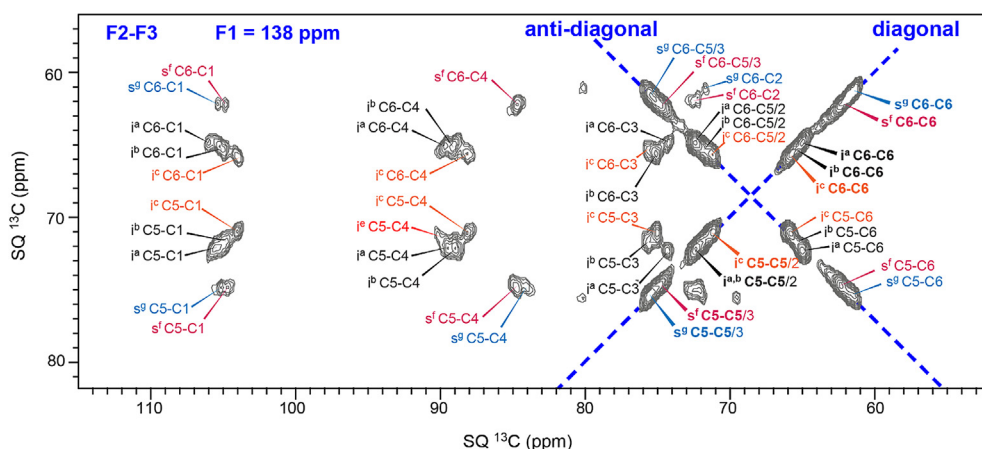


**Fig. 6.** Diagonal and antidiagonal signals of F2-F3 planes. Resonance assignment is shown for a F2-F3 plane (F1 = 138 ppm; cellulose C5-C6) extracted from the 3D spectrum of the spruce sample. Dashlines show the positions of the diagonal and anti-diagonal cross peaks. The assignments of the diagonal peaks are highlighted in bold.

molecules, are both tightly associated with the internal chains. While only a single F2-F3 plane is shown here to demonstrate the technical feasibility, the full long-range correlation 3D spectrum carries a rich pool of data that could possibly revise our understanding of the structure and bundling of cellulose, as well as its interactions with matrix polysaccharides.

Both the fungal and plant samples studied here are never-dried materials. The native hydration level is also key to the spectral resolution because the hydration state is particularly important for the mobile and non-crystalline components that rely on motional dynamics to narrow the lines. Fortunately, most carbohydrates

could efficiently retain their associations with water molecules. Three recent studies conducted on the primary and secondary plant cell walls as well as the microalgal cells have demonstrated that the <sup>13</sup>C resolution of cell wall carbohydrates is largely independent of the hydration history of the sample and can be fully restored upon rehydration [27,42,43]. However, irreversible changes might occur to the nanostructure of water-stabilized biopolymer interface upon dehydration [44,45]. Therefore, the sample preparation procedures, in addition to the spectroscopic methods, should be carefully designed and tested to ensure sufficient resolution for investigating carbohydrate-rich biomaterials.

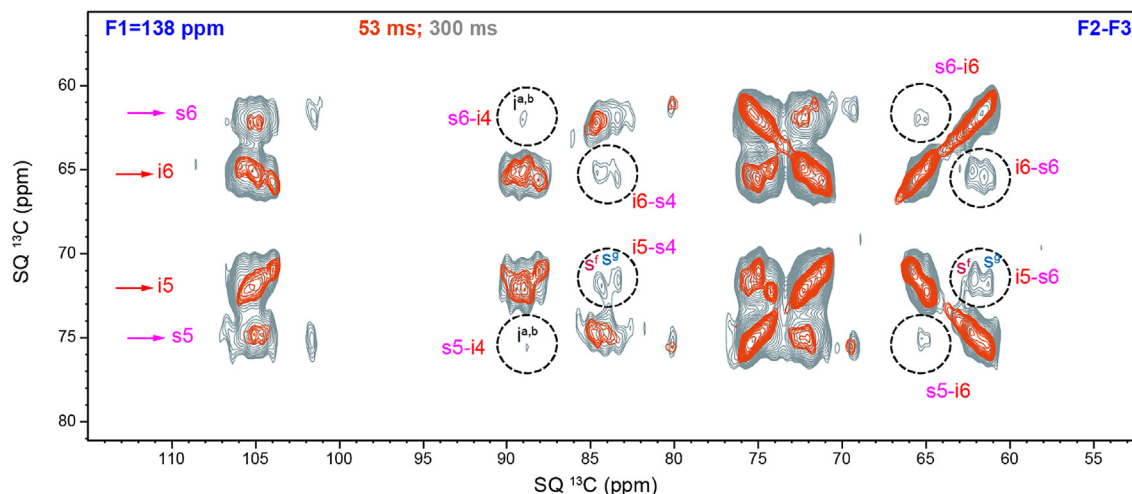


**Fig. 7.** Long-range intermolecular interactions in spruce cellulose. The comparison of F2-F3 planes ( $F1 = 138$  ppm) showed numerous long-range intermolecular cross peaks (overlaid with short range spectra in red). The key interactions between internal and surface chains of cellulose are selectively highlighted using dash line circles. Within each circle, the signals of different types of glucose units can be unambiguously resolved, yielding site- and conformer-specific information on the chain packing of cellulose.

### 3. Conclusions

Because the current solid-state NMR investigations of complex carbohydrates heavily rely on  $^{13}\text{C}$  detection, the resolution improvement provided by this 3D DQ-SQ-SQ correlation experiment has significantly expanded our technical capability. This study has demonstrated the unambiguous assignment of all carbon signals in the chitin and glucans of fungal cell walls. The spectra have also shown sufficient resolution for investigating cellulose and matrix polysaccharides in plant biomass. This 3D CCC approach could become a standard experiment for future investigations of the polymorphic structure and spatial association of carbohydrates in cellular systems and functional biomaterials [46]. Inclusion of novel homonuclear recoupling and third-spin-assisted recoupling methods [47–49] as well as the introduction of underexplored nuclei (such as  $^1\text{H}$ ,  $^2\text{H}$ ,  $^{15}\text{N}$ ,  $^{17}\text{O}$ , and  $^{19}\text{F}$ ) [18–20,50–53] might further extend the use of 3D experiments in carbohydrate solid-state NMR research.

### 4. Materials and methods

#### 4.1. Sample preparation

Three uniformly  $^{13}\text{C}$ -labeled samples were used in this study, including the intact cells of *A. fumigatus* (also with uniform  $^{15}\text{N}$ -labeling), the never-dried stems of spruce, and the model tripeptide formyl-Met-Leu-Phe-OH (MLF). For both *A. fumigatus* and spruce, around 35–40 mg of materials were packed into 3.2 mm pencil rotors. In addition, 7 mg of MLF was center packed into a 4 mm rotor. The fungal sample was freshly prepared following previously established protocols [33,34,39]. Briefly, the mycelium of *A. fumigatus* was obtained by growing the wild-type strain (RL 578) in a minimum liquid medium containing  $^{13}\text{C}$ -glucose (10.0 g/L) and  $^{15}\text{N}$ -sodium nitrate (6.0 g/L). The culture was incubated at 30 °C for 3 days under 210 rpm shaking condition. The material was then harvested by centrifugation (7,000g; 20 mins), and the resulting pellet was washed using 10 mM phosphate buffer (pH 7.4). The  $^{13}\text{C}$ -spruce sample was acquired from Isolife (the Netherlands), with the stems debarked manually. The wood material was hand-grinded using a pestle and a mortar to achieve relatively uniform size for the pieces in the range of a few millimeters across.

#### 4.2. Experiments

The 3D experiment was first verified using MLF on a 400 MHz (9.4 Tesla) using a 4.0 mm probe under 10 kHz MAS. The CORD mixing was 53 ms for the 3D experiment. The recycle delay was 1.6 s, and 8 scans were collected. The acquisition time was 15 ms, 7.0 ms, and 5.2 ms for the F3, F2, and F1, respectively (with respective spectral widths of 497, 99, and 80 ppm). The F2 and F1 dimensions have 140 and 84 points (70 and 42 complex points), respectively. The total experimental time was 43 h. The F2-F3 planes showed good resolution of all carbon sites as demonstrated in Supplementary Fig. 3.

Both the *A. fumigatus* and spruce samples were measured on an 800 MHz NMR (18.8 Tesla) Bruker Avance III HD spectrometer at the National High Magnetic Field Laboratory (NHMFL) using a 3.2 mm Low-E HCN probe designed and constructed in-house. The experiments were conducted under 13.5 kHz MAS at 293 K. The  $^{13}\text{C}$  chemical shifts were externally referenced to the tetramethylsilane (TMS) scale. The typical radiofrequency field strengths were 83 kHz for  $^1\text{H}$  decoupling and pulses, and 62.5 kHz for  $^{13}\text{C}$  pulses.

A 53-ms CORD recoupling time was used for the 3D experiment of *A. fumigatus*. The spectral widths were set to 497 ppm, 68 ppm, and 66 ppm for the F3, F2, and F1, respectively. The acquisition time was chosen to be 15 ms (F3), 6.0 ms (F2), and 6.0 ms (F1). This corresponds to 164 and 160 slices for the F2 and F1 dimensions. The recycle delay was 1.1 s, and 16 scans were collected. The total experimental time was 134 h.

Two INADEQUATE-CORD spectra were collected using the spruce sample, with short (53 ms) and long (300 ms) CORD mixing. Both 3D experiments used spectral widths of 497 ppm, 62 ppm, and 70 ppm for the F3, F2, and F1, respectively. The short-mixing 3D spectrum has acquisition times of 15 ms, 4.1 ms, and 4.1 ms for the F3, F2, and F1, respectively. These values correspond to 102 and 116 slices for the F2 and F1 dimensions. The short-mixing 3D spectrum was collected using 32 scans and 1 s recycle delays, with a total experimental time of 110 h. The number of scans was doubled for the long-mixing 3D spectrum for better signal-to-noise ratios, which is the barrier for observing the weak long-range cross peaks. The recycle delay was further shortened to 0.93 s. The F2 and F1 dimensions have 74 and 84 slices, respectively. The total experimental time for the long-mixing 3D was 136 h. For each sample, two collapsed 2D spectra of the F1-F3

and F2-F3 dimensions were measured separately using identical parameters as used in the 3D experiments.

### Declaration of Competing Interest

The authors declare that they have no known competing financial interests or personal relationships that could have appeared to influence the work reported in this paper.

### Acknowledgments

This work was supported by the National Science Foundation MCB-1942665. The National High Magnetic Field Laboratory is supported by National Science Foundation through NSF/DMR-1644779 and the State of Florida.

### Appendix A. Supplementary material

Supplementary data to this article can be found online. The supplementary data contains the full F2-F3 planes of *A. fumigatus* 3D spectra, the 3D spectra of spruce, demonstrative spectra of MLF, and the NMR pulse program of the 3D INADEQUATE-CORD experiment.

Supplementary data to this article can be found online at <https://doi.org/10.1016/j.jmr.2022.107148>.

### References

- J. Pauli, M. Baldus, B. van Rossum, H. de Groot, H. Oschkinat, Backbone and side-chain  $^{13}\text{C}$  and  $^{15}\text{N}$  signal assignments of the a-Spectrin SH3 domain by magic angle spinning solid-state NMR at 17.6 Tesla, *ChemBioChem* 2 (2001) 272–281.
- B. Reif, S.E. Ashbrook, L. Emsley, M. Hong, Solid-state NMR spectroscopy, *Nat. Rev. Methods Primers* 1 (2021) 2.
- J. Hoffmann et al., Protein resonance assignment by BSH-CP-based 3D solid-state NMR experiments: A practical guide, *Magn. Reson. Chem.* 58 (2020) 445–465.
- H. Heise, K. Seidel, M. Etzkorn, S. Becker, M. Baldus, 3D NMR spectroscopy for resonance assignment and structure elucidation of proteins under MAS: novel pulse schemes and sensitivity considerations, *J. Magn. Reson.* 173 (2005) 64–74.
- D. Zhou, K.D. Kloepper, K.A. Winter, C.M. Rienstra, Band-selective  $^{13}\text{C}$  homonuclear 3D spectroscopy for solid proteins at high field with rotor-synchronized soft pulses, *J. Biomol. NMR* 34 (2006) 245–257.
- S. Li, Y. Zhang, M. Hong, 3D  $^{13}\text{C}$ - $^{13}\text{C}$  correlation NMR for De Novo distance determination of solid proteins and application to a human alpha defensin, *J. Magn. Reson.* 202 (2010) 203–210.
- A.J. Dregni et al., In vitro ON4R tau fibrils contain a monomeric  $\beta$ -sheet core enclosed by dynamically heterogeneous fuzzy coat segments, *Proc. Natl. Acad. Sci. USA* 116 (2019) 16357–16366.
- M.J. Duer, The contribution of solid-state NMR spectroscopy to understanding biomineralization: atomic and molecular structure of bone, *J. Magn. Reson.* 253 (2015) 98–110.
- M. Dick-Pérez et al., Structure and interactions of plant cell-wall polysaccharides by two- and three-dimensional magic-angle-spinning solid-state NMR, *Biochemistry* 50 (2011) 989–1000.
- R. Dupree et al., Probing the molecular architecture of arabidopsis thaliana secondary cell walls using two- and three-dimensional  $^{13}\text{C}$  solid state nuclear magnetic resonance spectroscopy, *Biochemistry* 54 (2015) 2335–2345.
- D.J. Cosgrove, Re-constructing our models of cellulose and primary cell wall assembly, *Curr. Opin. Plant Biol.* 22 (2014) 122–131.
- Y. Zhang et al., Molecular insights into the complex mechanics of plant epidermal cell walls, *Science* 372 (2021) 706–711.
- Y.B. Park, D.J. Cosgrove, A revised architecture of primary cell walls based on biomechanical changes induced by substrate-specific endoglucanases, *Plant Physiol.* 158 (2012) 1933–1943.
- J. Struppe et al., Expanding the horizons for structural analysis of fully protonated protein assemblies by NMR spectroscopy at MAS frequencies above 100 kHz, *Solid State Nucl. Magn. Reson.* 87 (2017) 117–125.
- L.B. Andreas et al., Structure of fully protonated proteins by proton-detected magic-angle spinning NMR, *Proc. Natl. Acad. Sci. USA* 113 (2016) 9187–9192.
- Y. Su, L. Andreas, R.G. Griffin, Magic Angle Spinning NMR of Proteins: High-Frequency Dynamic Nuclear Polarization and  $^1\text{H}$  Detection, *Annu. Rev. Biochem.* 84 (2015) 465–497.
- E.G. Keeler et al., High-Resolution  $^{17}\text{O}$  NMR Spectroscopy of Structural Water, *J. Phys. Chem. B* 123 (2019) 3061–3067.
- P. Phyo, M. Hong, Fast MAS  $^1\text{H}$ - $^{13}\text{C}$  correlation NMR for structural investigations of plant cell walls, *J. Biomol. NMR* 73 (2019) 661–674.
- C. Bougault, I. Ayala, W. Vollmer, J.P. Simorre, P. Schanda, Studying intact bacterial peptidoglycan by proton-detected NMR spectroscopy at 100 kHz MAS frequency, *J. Struct. Biol.* 206 (2019) 66–72.
- T.H. Sefzik et al., Solid-state  $^{17}\text{O}$  NMR in carbohydrates, *Chem. Phys. Lett.* 434 (2007) 312–315.
- S. Cadars et al., The refocused INADEQUATE MAS NMR experiment in multiple spin-systems: Interpreting observed correlation peaks and optimising lineshapes, *J. Magn. Reson.* 188 (2007) 24–34.
- S. Cadars, A. Lesage, L. Emsley, Chemical Shift Correlations in Disordered Solids, *J. Am. Chem. Soc.* 127 (2005) 4466–4476.
- G. Hou et al., Spin diffusion driven by R-symmetry sequences: applications to homonuclear correlation spectroscopy in MAS NMR of biological and organic solids, *J. Am. Chem. Soc.* 133 (2011) 3943–3953.
- G. Hou, S. Yan, J. Trébosc, J.-P. Amoureux, T. Polenova, Broadband homonuclear correlation spectroscopy driven by combined  $\text{R}_2^y$  sequences under fast magic angle spinning for NMR structural analysis of organic and biological solids, *J. Magn. Reson.* 232 (2013) 18–30.
- G.D. Brown et al., Hidden killers: human fungal infections, *Sci. Transl. Med.* 4 (2012).
- J.-P. Latgé, G. Chamilos, *Aspergillus fumigatus* and Aspergillosis in 2019, *Clin. Microbiol. Rev.* 33 (2019) e00140–00118.
- A. Poulhazan et al., Identification and quantification of glycans in whole cells: architecture of microalgal polysaccharides described by solid-state nuclear magnetic resonance, *J. Am. Chem. Soc.* 143 (2021) 19374–19388.
- J.E. Kelly, C. Chrissian, R.E. Stark, Tailoring NMR experiments for structural characterization of amorphous biological solids: A practical guide, *Solid State Nucl. Magn. Reson.* 109 (2020) 101686.
- N. Ghassemi, et al., Solid-State NMR Investigations of Extracellular Matrices and Cell Walls of Algae, Bacteria, Fungi, and Plants. *Chem. Rev.*, in press (2022). DOI: 10.1021/acs.chemrev.1c00669
- W. Thongsomboon et al., Phosphoethanolamine cellulose: A naturally produced chemically modified cellulose, *Science* 359 (2018) 334–338.
- S.A. Overall, A.B. Barnes, Biomolecular perturbations in in-cell dynamic nuclear polarization experiments, *Front. Mol. Biosci.* 8 (2021) 743829.
- R. Ghosh, Y. Xiao, J. Kragelj, K.K. Frederick, In-cell sensitivity-enhanced NMR of intact living mammalian cells, *J. Am. Chem. Soc.* 143 (2021) 18454–18466.
- X. Kang et al., Molecular architecture of fungal cell walls revealed by solid-state NMR, *Nat. Commun.* 9 (2018) 2747.
- A. Chakraborty et al., A molecular vision of fungal cell wall organization by functional genomics and solid-state NMR, *Nat. Commun.* 12 (2021) 6346.
- J.-P. Latgé, A. Beauvais, G. Chamilos, The Cell Wall of the Human Fungal Pathogen *Aspergillus fumigatus*: Biosynthesis, Organization, Immune Response, and Virulence, *Annu. Rev. Microbiol.* 71 (2017) 99–116.
- J.-P. Latgé, The cell wall: a carbohydrate armour for the fungal cell, *Mol. Microbiol.* 66 (2007) 279–290.
- M.J. Lee, D.C. Sheppard, Recent advances in the understanding of the *Aspergillus fumigatus* cell wall, *J. Microbiol.* 54 (2016) 232–242.
- A. Gastebois, C. Clavaud, V. Aïmanianda, J.-P. Latgé, *Aspergillus fumigatus*: cell wall polysaccharides, their biosynthesis and organization, *Future Microbiol.* 4 (2009) 583–595.
- L.D. Fernando et al., Structural Polymorphism of Chitin and Chitosan in Fungal Cell Walls from Solid-State NMR and Principal Component Analysis, *Front. Mol. Biosci.* 8 (2021) 727053.
- T. Wang, H. Yang, J.D. Kubicki, M. Hong, Cellulose structural polymorphism in plant primary cell walls investigated by high-field 2D solid-state NMR spectroscopy and density functional theory calculations, *Biomacromolecules* 17 (2016) 2210–2222.
- P. Phyo, T. Wang, Y. Yang, H. O'Neill, M. Hong, Direct determination of hydroxymethyl conformations of plant cell wall cellulose using  $^1\text{H}$  polarization transfer solid-state NMR, *Biomacromolecules* 19 (2018) 1485–1497.
- T. Wang, Y.B. Park, D.J. Cosgrove, M. Hong, Cellulose-pectin spatial contacts are inherent to never-dried *Arabidopsis* primary cell walls: evidence from solid-state nuclear magnetic resonance, *Plant Physiol.* 168 (2015) 871–884.
- Kirui, A. et al. Carbohydrate-Aromatic Interface and Molecular Architecture of Lignocellulose. *Nat. Commun.* 13, 538 (2022).
- R. Cresswell et al., Importance of Water in Maintaining Softwood Secondary Cell Wall Nanostructure, *Biomacromolecules* 22 (2021) 4669–4680.
- Y. Gao, A.S. Lipton, Y. Wittmer, D.T. Murray, J.C. Mortimer, A grass-specific cellulose-xylan interaction dominates in sorghum secondary cell walls, *Nat. Commun.* 11 (2020) 1–10.
- M.E. Hariri El Nokab, P.C.A. van der Wel, Use of Solid-state NMR spectroscopy for Investigating Polysaccharide-based Hydrogels: A Review, *Carbohydr. Polym.* 240 (2020) 116276.
- M.D. Gelenter, A.J. Dregni, M. Hong, Pulsed Third-Spin-Assisted Recoupling NMR for Obtaining Long-Range  $^{13}\text{C}$ - $^{13}\text{C}$  and  $^{15}\text{N}$ - $^{13}\text{C}$  Distance Restraints, *J. Phys. Chem. B* 124 (2020) 7138–7151.
- S. Paul, H. Takahashi, S. Hediger, G. De Paepe, Third Spin-Assisted Recoupling in SSNMR: Theoretical Insights and Practicable Application to Biomolecular Structure Determination, *Ann. Reports NMR Spectrosc.* 85 (2015) 93–142.
- G.D. Paëpe, J.R. Lewandowski, A. Loquet, A. Böckmann, R.G. Griffin, Proton assisted recoupling and protein structure determination, *J. Chem. Phys.* 129 (2008) 245101.

- [50] G. Wu,  $^{17}\text{O}$  NMR studies of organic and biological molecules in aqueous solution and in the solid state, *Progr. Nucl. Magn. Resonance Spectrosc.* 114 (2019) 1335-1191.
- [51] J.H. Fritz et al., Measurement of accurate interfluorine distances in crystalline organic solids: a high-frequency magic angle spinning NMR approach, *J. Phys. Chem. B* 123 (2019) 10680-10690.
- [52] A.A. Shcherbakov, J. Medeiros-Silva, N. Tran, M.D. Gelenter, M. Hong, From angstroms to nanometers: measuring interatomic distances by solid-state NMR, *Chem. Rev.*, in press. (2021).
- [53] M.D. Gelenter, T. Wang, S.-Y. Liao, H. O'Neill, M. Hong,  $^2\text{H}$ - $^{13}\text{C}$  correlation solid-state NMR for investigating dynamics and water accessibilities of proteins and carbohydrates, *J. Biomol. NMR* 68 (2017) 257-270.